Electrochemistry Communications 46 (2014) 111–114

Contents lists available at ScienceDirect

Electrochemistry Communications

journal homepage: www.elsevier.com/locate/elecom

Short communication

A gradient porous cathode for non-aqueous lithium-air batteries leading to a high capacity

P. Tan, W. Shyy, L. An, Z.H. Wei, T.S. Zhao *

Department of Mechanical and Aerospace Engineering, The Hong Kong University of Science and Technology, Clear Water Bay, Kowloon, Hong Kong, China

ARTICLE INFO

Article history:
Received 1 May 2014
Received in revised form 10 June 2014
Accepted 27 June 2014
Available online 5 July 2014

Keywords:
Lithium-air battery
Discharge capacity
Gradient pore distribution
Oxygen transport

ABSTRACT

In conventional porous cathodes of non-aqueous lithium-air batteries, the higher discharge reaction rate in the oxygen richer region will result in a gradient distribution of the solid product, Li_2O_2, decreasing from the air side to the separator side. Such a distribution of the solid product means that although the pores toward the separator side remain open, the pores at the air side will be blocked first with an increase in the discharge capacity, terminating the discharge process and resulting in a low discharge capacity. In this work, we design and fabricate a cathode structure with a stepwise gradient pore distribution (pore size reducing from 500 to 300 and 100 nm) by mixing carbon powder and nanotubes. The gradient porous cathode enables the capacity of a non-aqueous lithium-air battery discharging at 0.1 mA/cm^2 to be 19.2% higher than that by a uniform porous cathode (~100 nm in pore size) and 82.3% higher than that by a uniform porous cathode (~500 nm in pore size). The SEM image analysis suggests that the increased discharge capacity can be mainly attributed to the fact that the gradient cathode can not only increase oxygen transport pathways but also retain a sufficiently large specific surface area.

1. Introduction

Non-aqueous lithium-air batteries have been considered as one of the most promising power sources for next-generation electric vehicles and portable devices [1], due to the super high theoretical capacity (3.86×10^3 mA h/g) and energy density (1.14×10^4 W h/kg), which is several times higher than that of Li-ion batteries [2,3]. It has been shown, however, that the actual discharge capacity is much lower than the theoretical value. In addition to the instability of electrolyte and electrode materials [4–8], a key factor that limits the actual capacity is related to the formation of Li_2O_2 during discharge [9], which is insoluble in the non-aqueous electrolyte and deposits in the void spaces of the porous cathode. The oxygen concentration in the porous cathode decreases from the air side to the separator side during discharge. In the initial discharge period, the oxidation reaction is predominately controlled by the transport of oxygen. Higher oxygen concentration will result in a higher reaction rate. Hence, the fraction of the solid product will be larger at the air side, decreasing toward the separator side [10–14]. Such a distribution of the solid product means that although the remaining pores toward the separator side are still open, the pores at the air side will be blocked first with an increase in the discharge capacity, terminating the discharge process and resulting in a low discharge capacity. In the meantime, due to the low electric conductivity of Li_2O_2 [15], increased electric resistance with the growth of solid product films can also terminate discharge. Therefore, in a uniform porous cathode, the transport limit of either oxygen or electrons resulting from the grown solid product size at the air side will terminate the discharge process before the surface area and void volume are fully utilized, leading to a capacity much lower than the theoretical value.

The above-mentioned issue can be addressed by forming a porous cathode with a gradient distribution in pore size. The implementation of such a gradient will enable a more even oxygen transport pathway along the electrode thickness. It has been numerically demonstrated that the gradient cathode can increase the discharge capacity [12]. In this work, we fabricate a cathode structure with a stepwise gradient pore distribution by mixing carbon powder and nanotubes. The application of this gradient porous cathode was tested in a non-aqueous lithium-air battery, and compared with the uniform porous cathode made of pure carbon powder and nanotubes. The cathode morphology after discharge was examined, and the correlation between the discharge capacity and oxygen transport was studied.

2. Experimental

2.1. Cathode fabrication

The proposed stepwise-gradient porous cathode was formed by binding three layers with different pore sizes. The separator-side layer (interfaced with the separator), the densest layer, was formed in three steps: i) mixing carbon powder with polytetrafluorethylene (PTFE) (as the binder) at a weight ratio of 8:2; ii) adding ethanol as a dispersing

* Corresponding author. Tel.: +852 2358 8647.
E-mail address: metzhao@ust.hk (T.S. Zhao).

http://dx.doi.org/10.1016/j.elecom.2014.06.026
1388-2481/

agent to form slurry, which was ultrasonically stirred for 1 h; and iii) air-drying the mixture to be rolled to form the layer with a thickness of 250 μm. The air-side layer (facing the air) was the loosest layer, having the same thickness as the separator-side layer, and was composed of pure carbon nanotubes and formed by following the same procedures as that for the formation of the separator-side layer. The middle layer, also 250 μm thick, was formed by mixing carbon powder and nanotubes at the weight ratio of 1:1. To bind the three layers together, a thin slurry layer of mixed carbon powder and nanotubes at the weight ratio of 1:1 with PTFE was painted onto both sides of the middle layer. Subsequently, the three layers were combined together, rolled, baked at 240 °C and sintered at 350 °C, for 1 h each, to form the electrode of 750 μm in thickness. Finally, the electrode was cut to form a circular shape with 10 mm in diameter. For the purpose of comparison, another two electrodes made of pure carbon powder (CP) and carbon nanotubes (CNT), respectively, with 750 μm in thickness and 10 mm in diameter were also prepared. The carbon loadings in the gradient and uniform porous cathodes made of CP and CNT are 14.4, 13.1, and 16.8 mg, respectively.

The specifications of the carbon materials used to form the electrodes are as follows. Carbon powder (Ketjen Black EC-600JD, AkzoNobel Co. Ltd., Asia) is approximately 20 nm in diameter and 1334 m^2/g in the specific surface area, while multi-walled carbon nanotubes (Shenzhen Nanotech Co. Ltd., China) are 40 to 60 nm in diameter, 5 to 15 μm in length, and 49 m^2/g in the specific surface area.

2.2. Performance tests and characterizations

The discharge performance of the cathodes was tested in a non-aqueous lithium-air battery that consisted of a lithium foil anode, a glass-fiber separator (Whatman GF/C), and 250 μL 1 M LiTFSI (Sigma-Aldrich, 99.95%) in TEGDME (Sigma-Aldrich, 99%) as the electrolyte to fully saturate the cathode. The entire battery was assembled in an argon-filled glove box (Etelux, Lab 2000) at water and oxygen contents below 1 ppm. All tests were performed at room temperature (25 °C) at the constant oxygen pressure of 1 atm by the battery cycling system (Neware, CT-3008W).

The microscopic structure of the cathode was observed by a scanning electron microscope (SEM, JEOL Inc., JSM-6300) under an acceleration voltage of 20 kV. The discharge product composition was analyzed by a Philips high resolution X-ray diffraction system (XRD, model PW 1825) using a Cu-Kα source operating at 40 keV.

3. Results and discussion

Fig. 1a shows the cross section of the gradient porous cathode. It is seen that the three layers are well interfaced. The microscopic structure images of the three layers are respectively shown in Fig. 1b–d. In the layer with the highest porosity (the air-side layer), carbon nanotubes are weaved to form large pores of about 500 nm. In the middle layer, the addition of carbon powder to nanotubes results in pores that are smaller (around 300 nm) than those in the air-side layer. In the separator-side layer, spherical carbon powder particles are connected tightly to form relatively small pores, around 100 nm in size. As illustrated in Fig. 1a, the cathode has a stepwise distribution in pore size, decreasing from 500 to 300 and 100 nm towards the separator side. In contrast, the cathodes made of CP and CNT show a relatively uniform pore size, respectively, at 100 and 500 nm.

The discharge voltage curves for gradient and uniform porous cathodes at small (0.1 mA/cm^2) and large (0.5 mA/cm^2) current densities are shown in Fig. 2a and b. In both cases, the voltage plateaus of the gradient porous cathode are lower than that of the uniform porous cathode (~100 nm in pore size), but higher than that of the uniform porous cathode (~500 nm in pore size). This is mainly attributed to the difference in the cathodic reaction area, resulting from the fact that the specific area of CNT is much smaller than that of CP. It is interesting to notice that the discharge capacity of the gradient porous cathode is the highest among three cases. At 0.1 mA/cm^2, the capacity is 38.88 mA h/cm^2 (2120 mA h/g), which is 19.2% and 82.3% higher than that of the

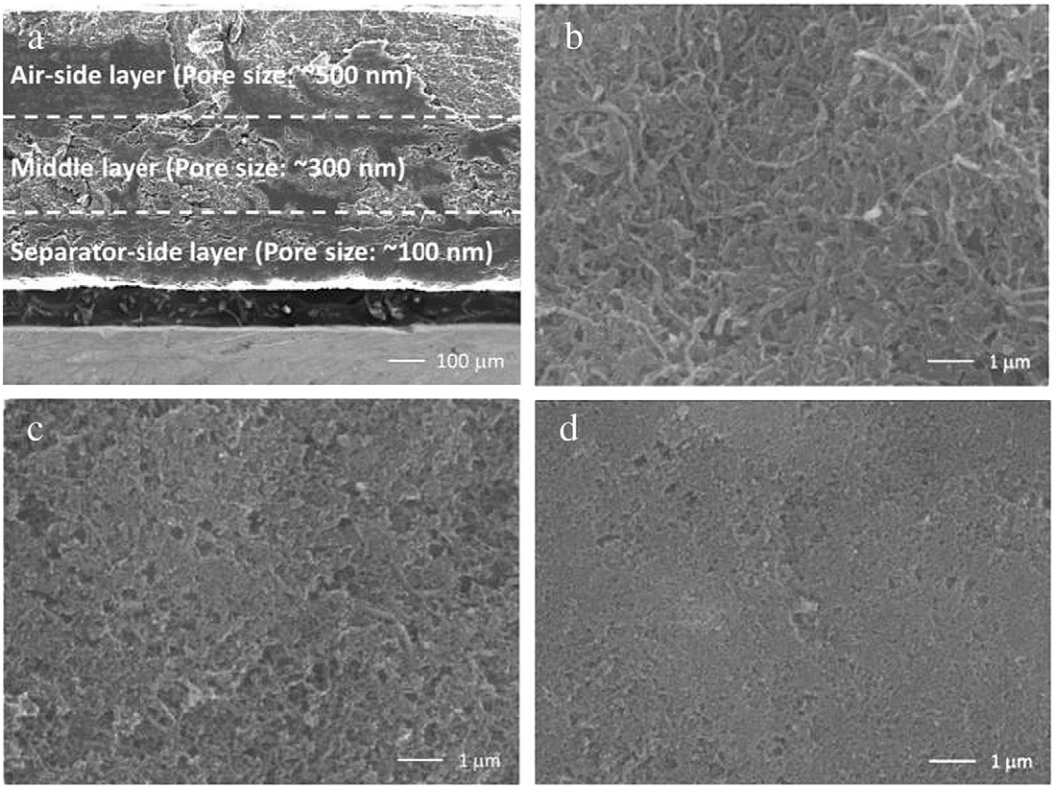

Fig. 1. SEM image of (a) the cross section of the gradient porous cathode (50×); (b–d) microscopic structure of the air-side, middle, and separator-side layer, respectively (10,000×).

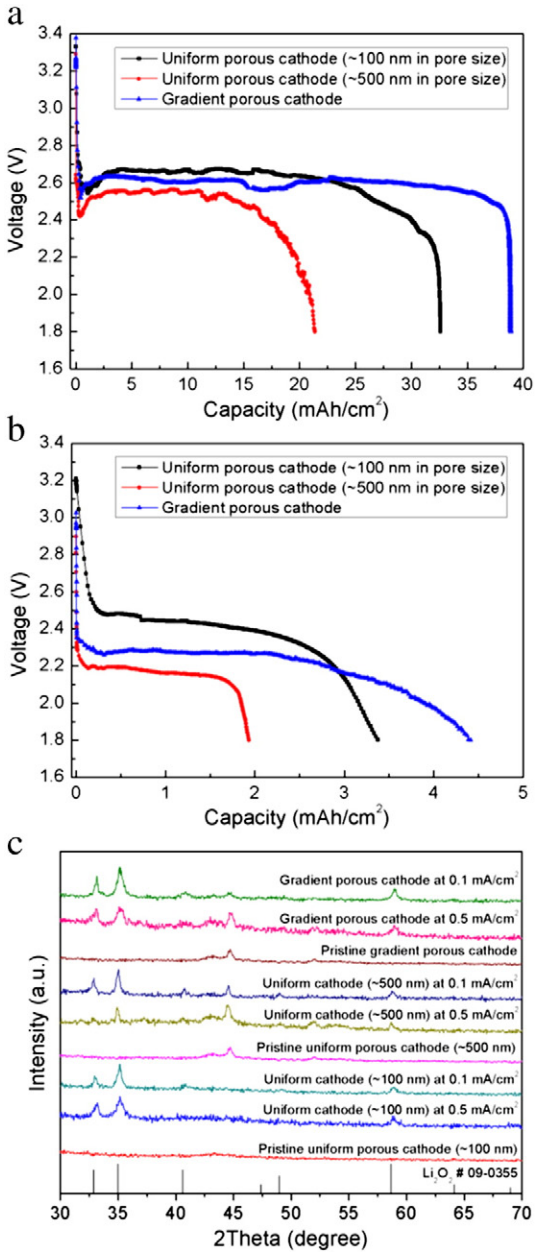

Fig. 2. (a–b) Galvanostatic discharge curves at 0.1 and 0.5 mA/cm^2, respectively; (c) XRD patterns of the cathodes before and after discharge and the reference patterns according to JCPDS database.

uniform porous cathode with ~100 and ~500 nm in pore size, respectively. While at 0.5 mA/cm^2, the capacity is 4.58 mA h/cm^2 (250 mA h/g), with an increment by 35.8% and 140.0%, respectively. As for the specific capacity, the increment is 8.5% and 112.6% at 0.1 mA/cm^2, and 23.8% and 180.9% at 0.5 mA/cm^2, respectively. It is also worth noting that the XRD characterizations, shown in Fig. 2c, suggest that the discharge product is Li_2O_2.

To provide insight into the improved capacity of the gradient porous cathode, the morphology of each cathode is presented in Fig. 3. For the uniform porous cathode (~100 nm in pore size), both sides exhibit toroid-like products on the surface, and the particle sizes are larger at the separator-side than those at the air-side. Similar phenomenon could be observed in the uniform porous cathode with ~500 nm in pore size. We offer an explanation for this phenomenon: on one hand, the particle size is larger at a smaller current density [16]. On the other hand, the local current density depends on the oxygen concentration. Therefore, decreased oxygen concentration results in the decreased local current density from the air-side to the separator-side. This leads to the larger particle size at the separator-side. For the uniform porous cathode (~100 nm in pore size), the accumulation of product particles could easily block the small pores. Although increasing the pore size could enhance oxygen transport and thus improve the discharge capacity [17], it will meanwhile reduce the specific surface area and thus limit the discharge capacity, as evidenced by the result of the uniform porous cathode (~500 nm in pore size). For the gradient porous cathode, as shown in Fig. 3b, film-like products with large toroid-like products cover the carbon nanotube surface (air-side), whereas at the separator-side, numerous small product particles are distributed onto the carbon powder surface. The large amount of reduced-size products indicates that the oxygen concentration at the separator side was increased, as a result of the increased oxygen transport pathways along the electrode thickness. Meanwhile, a sufficiently large specific surface area was retained through the middle and separator layer. Therefore, a high discharge capacity was achieved.

4. Conclusions

In summary, we have designed and fabricated a triple-layer structured cathode with a stepwise gradient pore distribution for non-aqueous lithium-air batteries. The layer with the highest porosity facing the air-side was composed of carbon nanotubes, whereas the layer with the lowest porosity interfaced with the separator side was made of carbon powder. The middle layer was made of carbon nanotubes and

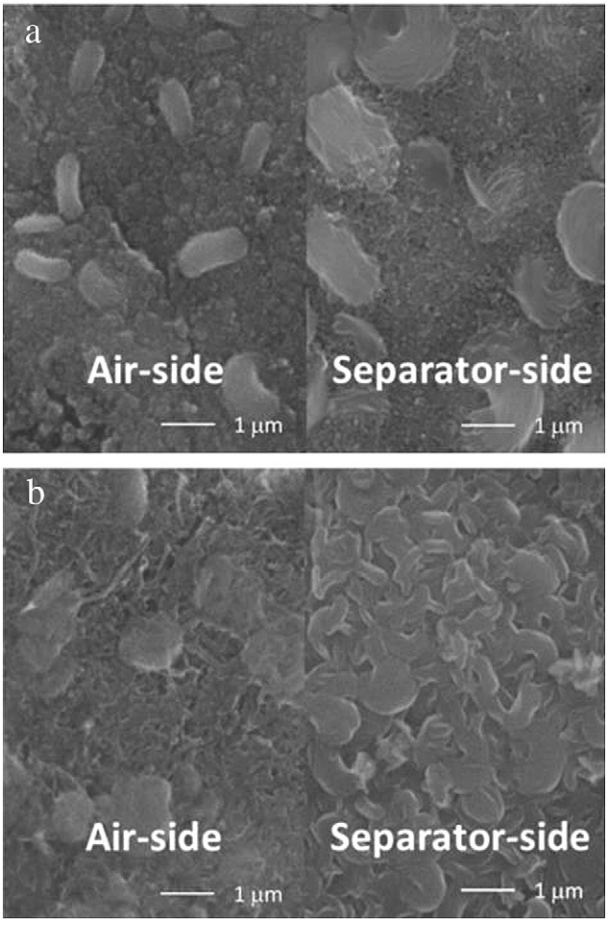

Fig. 3. SEM image of the cathode after discharge at the current density of 0.1 mA/cm^2 (10,000×): (a) uniform porous cathode (~100 nm in pore size); (b) gradient porous cathode.

powder at the weight ratio of 1:1. The gradient porous cathode with pore size reducing from 500 to 300 and 100 nm enables the capacity of a non-aqueous lithium-air battery discharging at 0.1 mA/cm^2 to be 19.2% and 82.3% higher than that by a uniform porous cathode with ~100 and ~500 nm in pore size, respectively. The SEM image analysis suggests that the increased discharge capacity can be mainly attributed to the fact that the gradient cathode can not only increase oxygen transport pathways but also retain a sufficiently large specific surface area. The significance of this work is that it has been practically demonstrated that a porous electrode with a gradient pore distribution is required for non-aqueous lithium-air batteries.

Conflict of interest

There is no conflict of interest.

Acknowledgments

The work described in this paper was fully supported by a grant from the Research Grants Council of the Hong Kong Special Administrative Region, China (Project No. 622712).

References

[1] G. Girishkumar, B. McCloskey, A.C. Luntz, S. Swanson, W. Wilcke, J. Phys. Chem. Lett. 1 (2010) 2193–2203.
[2] J.P. Zheng, R.Y. Liang, M. Hendrickson, E.J. Plichta, J. Electrochem. Soc. 155 (2008) A432–A437.
[3] P. Tan, Z. Wei, W. Shyy, T.S. Zhao, Appl. Energy 109 (2013) 275–282.
[4] C.J. Barile, A.A. Gewirth, J. Electrochem. Soc. 160 (2013) A549–A552.
[5] X. Guo, N. Zhao, Adv. Energy Mater. 3 (2013) 1413–1416.
[6] Z.H. Cui, W.G. Fan, X.X. Guo, J. Power, Sources 235 (2013) 251–255.
[7] B.D. McCloskey, A. Speidel, R. Scheffler, D.C. Miller, V. Viswanathan, J.S. Hummelshoj, J.K. Norskov, A.C. Luntz, J. Phys. Chem. Lett. 3 (2012) 997–1001.
[8] M.M. Ottakam Thotiyl, S.A. Freunberger, Z. Peng, P.G. Bruce, J. Am. Chem. Soc. 135 (2013) 494–500.
[9] Z. Peng, S.A. Freunberger, Y. Chen, P.G. Bruce, Science 337 (2012) 563–566.
[10] S.S. Sandhu, J.P. Fellner, G.W. Brutchen, J. Power, Sources 164 (2007) 365–371.
[11] P. Andrei, J.P. Zheng, M. Hendrickson, E.J. Plichta, J. Electrochem. Soc. 157 (2010) A1287–A1295.
[12] X. Li, A. Faghri, J. Electrochem. Soc. 159 (2012) A1747–A1754.
[13] U. Sahapatsombut, H. Cheng, K. Scott, J. Power, Sources 227 (2013) 243–253.
[14] G.Q. Zhang, J.P. Zheng, R. Liang, C. Zhang, B. Wang, M. Hendrickson, E.J. Plichta, J. Electrochem. Soc. 157 (2010) A953–A956.
[15] V. Viswanathan, K.S. Thygesen, J.S. Hummelshoj, J.K. Norskov, G. Girishkumar, B.D. McCloskey, A.C. Luntz, J. Chem. Phys. 135 (2011) 214704.
[16] B.D. Adams, C. Radtke, R. Black, M.L. Trudeau, K. Zaghib, L.F. Nazar, Energy Environ. Sci. 6 (2013) 1772–1778.
[17] C.N. Chervin, M.J. Wattendorf, J.W. Long, N.W. Kucko, D.R. Rolison, J. Electrochem. Soc. 160 (2013) A1510–A1516.